Controls of cross-shore planktonic ecosystem structure in Eastern Boundary Upwelling Systems

Jordyn E. Moscoso [1,2]*, Daniele Bianchi [2], Andrew L. Stewart [2]

[1]Department of Ocean Sciences, University of California, Santa Cruz, California, USA
[2]Department of Atmospheric and Oceanic Sciences, University of California, Los Angeles, California, USA

Key Points:

- An idealized quasi-2D model (MAMEBUS) of Eastern Boundary Upwelling Systems (EBUSs) and coupled size structured ecosystem model is presented
- Controls on the across-shore phytoplankton size structure are identified by a set of model experiments
- Idealized simulations configured to the California Current System (CCS) show wind stress maximum and nutrient concentration in upwelled water set zonal plankton size distributions

*Corresponding Author

Corresponding author: Jordyn E. Moscoso, jmoscoso@ucsc.edu

Abstract

Eastern boundary upwelling systems (EBUSs) are among the most productive regions in the ocean because deep, nutrient-rich waters are brought up to the surface. Previous studies have identified winds, mesoscale eddies and offshore nutrient distributions as key influences on the net primary production in EBUSs. However uncertainties remain regarding their roles in setting cross-shore primary productivity and ecosystem diversity. Here, we use a quasi-two-dimensional (2D) model that combines ocean circulation with a spectrum of planktonic sizes to investigate the impact of winds, eddies, and offshore nutrient distributions in shaping EBUS ecosystems. A key finding is that variations in the strength of the wind stress and the nutrient concentration in the upwelled waters control the distribution and characteristics of the planktonic ecosystem. Specifically, a strengthening of the wind stress maximum, driving upwelling, increases the average planktonic size in the coastal upwelling zone, whereas the planktonic ecosystem is relatively insensitive to variations in the wind stress curl. Likewise, a deepening nutricline shifts the location of phytoplankton blooms shore-ward, shoals the deep chlorophyll maximum offshore, and supports larger phytoplankton across the entire domain. Additionally, increased eddy stirring of nutrients suppresses coastal primary productivity via "eddy quenching", whereas increased eddy restratification has relatively little impact on the coastal nutrient supply. These findings identify the wind stress maximum, isopycnal eddy diffusion, and nutricline depth as particularly influential on the coastal ecosystem, suggesting that variations in these quantities could help explain the observed differences between EBUSs, and influence the responses of EBUS ecosystems to climate shifts.

Plain Language Summary

Ecosystems in Eastern Boundary Upwelling Systems (EBUSs) are supported by the movement of nutrient-rich water from the deep ocean to the coastal surface waters through a wind-driven process called "upwelling". Many factors can impact the across-shore (zonal) distribution of size in EBUSs, with abundant large phytoplankton near shore, and sparse small phytoplankton offshore. For example, the strength of the wind controls upwelling, the subsurface nutrient distribution determines surface nutrient supply, and large-scale ocean vortices ("eddies") remove nutrients from the surface. However, there remains uncertainty as to the relative importance of these different factors in determining the sizes and abundance of phytoplankton upwelling ecosystems. This study utilizes a physical ocean model coupled to an ecosystem model to investigate the impact of various physical and biological influences on planktonic ecosystems in EBUSs. We find that the strength of the wind, the mixing of nutrients by eddies, and the concentration of nutrients in the upwelled waters are most important in determining the ecosystem structure. In contrast, cross-shore variations in the wind and the tendency of eddies to push waters downward near the coast are less influential. Our findings provide clarity on how physical and biochemical aspects of the EBUS environment influence its ecosystem.

1 Introduction

Eastern Boundary Upwelling Systems (EBUSs) support productive and diverse biological communities (Chavez & Messié, 2009; Bakun & Parrish, 1982). The along-shore equatorward winds drive an offshore transport of surface water and resulting upwelling of dense, nutrient-rich water to the surface (Bakun & Nelson, 1991; M. Jacox & Edwards, 2012; M. J. Jacox & Edwards, 2011). At the same time, a complex interplay of physical phenomena that arise as a consequence of upwelling often works to redistribute and even subduct nutrients in a process known as "eddy quenching", which ultimately reduces surface productivity (Colas et al., 2013; Gruber et al., 2011). Understanding responses of the local food-web to these and other forms of variability in the physical en-

vironment is important for regional socioeconomic stability (Golden et al., 2016; Pozo Buil et al., 2021).

Ecological responses to wind-driven upwelling in EBUSs have long been studied (Messié et al., 2009; Van Oostende et al., 2018; Gruber et al., 2011; Renault et al., 2016), yet uncertainties remain in the response of ecosystem diversity and the regional structure of the food-web. While the location of phytoplankton blooms and biomass is predominantly set by the total nutrient supply and availability (Marañón et al., 2014), the controls on the zonal ecosystem composition in EBUSs are less clear. In regions of high productivity near the coast, large phytoplankton contribute to the plurality of the biomass (Sheldon et al., 1972; Hood et al., 1991; Taylor et al., 2012), whereas offshore in the deep chlorophyll maximum, small phytoplankton dominate the total biomass (Worden et al., 2004; Zubkov et al., 2000).

A variety of physical influences have been shown to be important in determining the structure of the food-web in EBUSs. This structure varies as a consequence of zonally variable nutrient variability, described as follows. The strength of the wind, which drives upwelling, combined with the subsurface nutrient concentration controls the total productivity in EBUSs. In general, with stronger upwelling associated with higher coastal surface productivity (Capet et al., 2004; Chavez & Messié, 2009; Rykaczewski & Dunne, 2010; Pozo Buil et al., 2021). Within our parameter space, we expect an increase in the overall strength of the wind to support higher phytoplankton biomass and larger cell sizes (Hood et al., 1991). However, studies have show that there exists a tradeoff in upwelling strength in productivity, with very strong upwelling reducing surface productivity Botsford et al. (2006).

While meridional equatorward winds drive bulk coastal upwelling and support productivity, they also generate a baroclinically unstable jet that sheds mesoscale eddies that restratify the water column, and transports nutrients and other tracers away from the euphotic zone, reducing productivity (Gruber et al., 2011; Colas et al., 2013; Capet et al., 2008).

Renault et al. (2016) found that the shape of the wind-stress curl controls the coastal flux of nutrients and net primary productivity in the euphotic zone, with a wider wind-stress curl associated with weaker "eddy quenching" and higher net primary production. As a consequence, EBUSs are characterized by a zonal gradient of productivity that spans several orders of magnitude between the coast and the oligotrophic open ocean. These differences in nutrient concentrations drive changes in ecosystem composition (Hood et al., 1991; Worden et al., 2004; Taylor et al., 2012). Eddy restratification, eddy stirring, and subduction have been suggested to reduce the total productivity at the surface and on the shelf (Renault et al., 2016; Colas et al., 2013). Thus, insofar as productivity and phytoplankton size are positively related (Van Oostende et al., 2018; Moscoso et al., 2022), an increase in eddy kinetic energy would work to decrease the size of plankton near the coast (Renault et al., 2016).

The composition of upwelled source waters also impacts the ecosystem structure. While physical controls can modulate the depth of the source water (M. J. Jacox & Edwards, 2011), the subsurface concentration of nutrients in the subtropics also impacts the nutrients that are upwelled (Pozo Buil et al., 2021). A shallow, sharp nutricline increases the amount of nutrients on the shelf, provided that the source depth of upwelled water does not change (M. Jacox & Edwards, 2012), and leads to an increase of productivity and plankton size near the coast.

Previous modeling work has been successful in capturing zonal patterns of phytoplankton productivity and size in regional frameworks. Goebel et al. (2010) shows a zonal transition from large plankton onshore to small plankton offshore in the California Current System (CCS) with an intermediate complexity biogeochemical model. Similarly,

Van Oostende et al. (2018) showed that a large diatom class was essential in capturing a near-shore surface chlorophyll maximum over an upwelling season in the Southern California Bight. Due to computational limitations of realistic, three-dimensional (3D) regional models, a systematic characterization of the responses of ecosystem diversity to biogeochemical and physical forcing in EBUSs is still lacking. Additionally, the factors that control the distribution of nutrients in EBUSs often co-vary. For example, eddies drive both restratification and advection along isopycnal surfaces, and are influenced by wind changes. These processes are hard to disentangle in complex, 3D eddy-resolving models. In contrast, the use of idealized models allows an independent exploration of the effects of individual model parameters, and can decouple the effects of physical processes that often co-vary in more complex regional models.

In this study, we conduct an expansive exploration of the ecological responses to upwelling under a wide parameter space. We configure an idealized quasi-2D Meridionally Averaged Model of Eastern Boundary Upwelling Systems (MAMEBUS, Moscoso et al. (2021); Stewart & Moscoso (2020)) to examine a large number of physical states representative of those found across the CCS. The physical model includes a finely-resolved size-structured ecosystem model (Moscoso et al., 2022; Banas, 2011; Ward et al., 2012) that represents the lower-trophic food-web cycling. Size-structured ecological models are often used to represent broad functional diversity in the food-web because size is generally an excellent proxy for other biological traits (Andersen et al., 2016), and are becoming common for global Earth system models (Ward et al., 2012; Henson et al., 2021; Negrete-García et al., 2022). In general, size-structured ecosystems with a fine resolution of the size dimension have not been studied in comprehensive regional and global models due to computational constraints. However, using a quasi-2D model, we are able to explore the behavior of a highly resolved planktonic food-web structure in an idealized framework.

The remainder of the paper is organized as follows: In Section 2, we describe the physical and biogeochemical model configurations, and discuss model parameters and their range. We additionally define model diagnostics used to identify the responses to perturbations in the model state. In Section 3, we present a reference solution focusing on ecosystem size structure and characteristics. In Section 4, we discuss the responses to variations across the parameter space in three sub-regions of an idealized EBUS to identify important controls. Finally, in Section 5, we discuss the results and their implications for ecosystem productivity and diversity in EBUSs.

2 Methods

The simulations presented in this study were conducted using a Meridionally Averaged Model of Eastern Boundary Upwelling Systems (MAMEBUS, Moscoso et al. (2021)), a quasi-2D idealized model coupled to a size-structured nutrient, phytoplankton, zooplankton, detritus (NPZD) model (Moscoso et al., 2022). A schematic of the main components of the model is shown in Figure 1. The physical setup of the model is similar to that presented in Moscoso et al. (2021); any differences in the model configuration are highlighted below.

2.1 Physical Model Configuration

We configure MAMEBUS to represent an idealized CCS in a quasi-2D framework. While 2D models have been used to investigate upwelling with respect to a wide physical parameter space in other studies of productivity in EBUSs (M. J. Jacox & Edwards, 2011; M. Jacox & Edwards, 2012), some of the 3D processes that have been shown to be important in controlling biological responses (Renault et al., 2016; Gruber et al., 2006) were not explicitly resolved. However, MAMEBUS includes a series of parameterizations that improve representation of these processes: The momentum equations are calculated

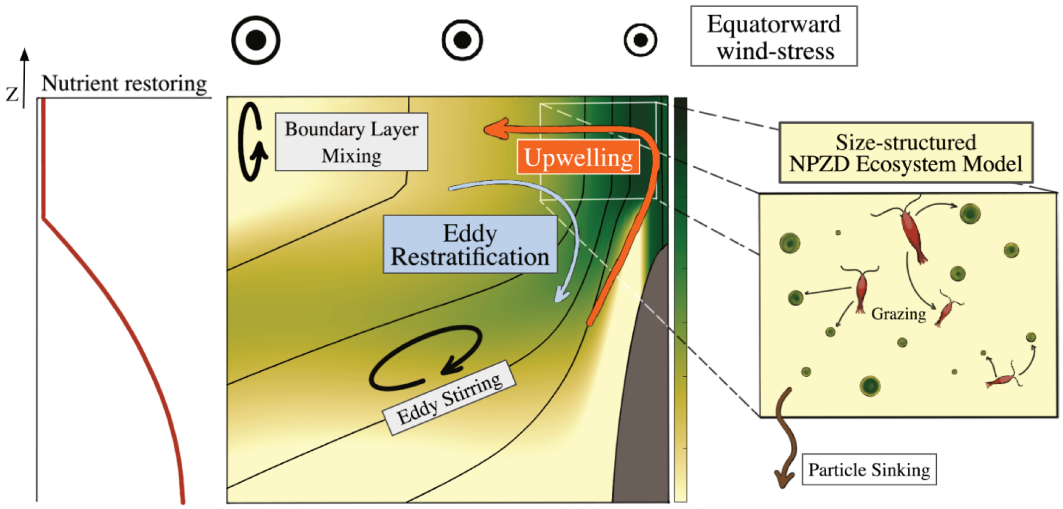

Figure 1: A schematic showing the major components of the coupled physical-biogeochemical model used in this study. Color contours in the central panel show total phytoplankton concentration, the black lines are isotherms, and the topography is shown in dark grey. The mean circulation is determined by wind-driven upwelling. Eddy restratification, eddy stirring, and boundary layer mixing are parameterized. Temperature and nutrients are restored to observed profiles at the western boundary, shown here in the left panel. The ecosystem component (right panel) consists of a size-structured ecosystem model with 50 phytoplankton and 50 zooplankton size classes.

following Dauhajre & McWilliams (2018). The effect of eddy restratification is parameterized following Gent & McWilliams (1990), eddy stirring along isopycnals is parameterized following Redi (1982) and surface and bottom boundary layer mixing is calculated following Ferrari et al. (2008). The detailed formulation of each of these parameterizations is described in Moscoso et al. (2021).

The physical design of MAMEBUS is meant to capture the broad behavior of upwelling in an idealized EBUS. Here, we configure the model to represent an idealization of the southern CCS. However this parameter space may encompass sections of parameter spaces found in other EBUSs. The model grid is cast in terrain-following coordinates. The model domain spans from the coast to 400 km offshore, and from the surface to 50m depth on the eastern (i.e., coastal) boundary of the domain, and 4000m depth on the western (i.e., open-ocean) boundary. At the eastern boundary, the shelf is prescribed to be deeper than what is found along the coast in order to reduce the model's computational time. The boundary conditions for temperature and nitrate at the western boundary are based on observations from The California Cooperative Oceanic Fisheries Investigations (CalCOFI) from Line 80 at Stations 90 and 100 from 1997 – 2018.

The topography is an idealized slope that follows ETOPO5 near Point Conception (Amante & Eakins, 2009), and slightly differs from that presented in Moscoso et al. (2021) by adopting a steeper slope to better represent the bathymetry near Point Conception, California (Line 80, CalCOFI). The model resolution is 60 horizontal grid-points and 60 vertical levels. This corresponds to an approximate grid-spacing of 6.7 km in the horizontal. MAMEBUS employs a stretched vertical coordinate, so the approximate vertical grid-spacing varies across the domain, from a minimum of 0.5 m near the coast to a maximum of $\sim$ 215 m at the western boundary.

The wind stress forcing is designed to approximate the median of monthly climatologies of data from ECMWF Reanalysis v5 (ERA5, Hersbach et al. (2020)) and from the Weather Research and Forecasting Model (WRF V4.1, Skamarock et al. (2008)) from 1997 – 2017. The along-shore component of the wind stress is calculated as an along-shore average from 34.5^{o}N to 35^{o}N, and shown as a function of distance from the coast over a 400km offshore extent for comparison to *in situ* data from Line 80 in CalCOFI data. This line is chosen because it falls between the latitudes where the data used for model configuration and forcing are averaged.

Specifically, the wind stress profile used in the model is given by:

$$\tau(x) = \tau_{\max} \tanh\left(\frac{L_x - x}{L_x/\tau_x}\right), \tag{1}$$

where $\tau_{\max}$ (N/m^2) is the wind stress maximum, L_x is the width of the model domain, and τ_x is a dimensionless tuning parameter that controls the width of the wind stress curl. Higher values of τ_x correspond to a narrower wind stress curl; however, the magnitude of the offshore wind stress does not change. The wind stress curl is given by $\partial_x \tau(x)$ (N/m^3). The reference wind stress profile is shown in Figure 2. In all instances of the model, described in Section 2.3, the wind-stress forcing is held constant. While there is substantial seasonality in the strength and shape of the wind across EBUSs Capet et al. (2004); Castelao & Luo (2018), we are interested in understanding the long-term steady-state behavior of the ecosystem, thus all physical forcing is constant.

To represent the offshore conditions that are set by processes occurring in the Pacific Ocean we define a 50km sponge layer on the western boundary of the domain. In this sponge layer, temperature and nitrate are restored to profiles that approximate *in situ* observations. The offshore temperature profile is defined as

$$T_R(z) = T_{\min} + (T_{\max} - T_{\min}) \cdot \left(\frac{\exp\left(\frac{z}{\Delta T_Z} + 1\right) - \exp\left(\frac{-H}{\Delta T_Z} + 1\right)}{\exp(1) - \exp\left(\frac{-H}{\Delta T_Z} + 1\right)}\right), \tag{2}$$

where $T_{\min}$ is the minimum temperature in the water column, $T_{\max}$ is the maximum temperature, ΔT_Z is the temperature decay scale, and $-H$ is the maximum depth of the water column. A reference buoyancy restoring profile is shown in Figure 3. At the surface, temperature is also restored to an idealized gradient based on observations from CalCOFI (see Moscoso et al. (2021)). The eastern boundary and the ocean floor have no flux boundary conditions.

2.2 Biogeochemical Model Configuration

MAMEBUS (Moscoso et al., 2021) is coupled online to a size structured NPZD model (SSEM, Moscoso et al. (2022)) based on previous work by Banas (2011) and Ward et al. (2012). Size is used as a proxy for ecological diversity, reflecting strong relationships between organism size and resource encounter strategies. This choice reduces the dimensionality of the model parameter space (compared to models which simulate multiple functional groups), while capturing important ecological behaviors (Follows & Dutkiewicz, 2011; Sauterey et al., 2017; Loeuille & Loreau, 2005; Banas, 2011). The size-dependent processes represented by the model include nutrient uptake by phytoplankton, heterotrophic grazing by zooplankton, predator-prey size interactions, plankton mortality, and size diffusion (i.e., mutation). Large phytoplankton have slow uptake rates, tend to be more nutrient limited, and have longer lifespans than their smaller counterparts (Tang, 1995; Eppley et al., 1969). The grazing dynamics are modeled under the assumption that small zooplankton quickly graze phytoplankton of approximately the same size, while large zooplankton prefer proportionally smaller prey, and have slower grazing rates (Hansen et al., 1994). However, this is an approximation that may not be representative of all zooplankton (Kiørboe, 2011). We parameterize phytoplankton mutations as a weak diffu-

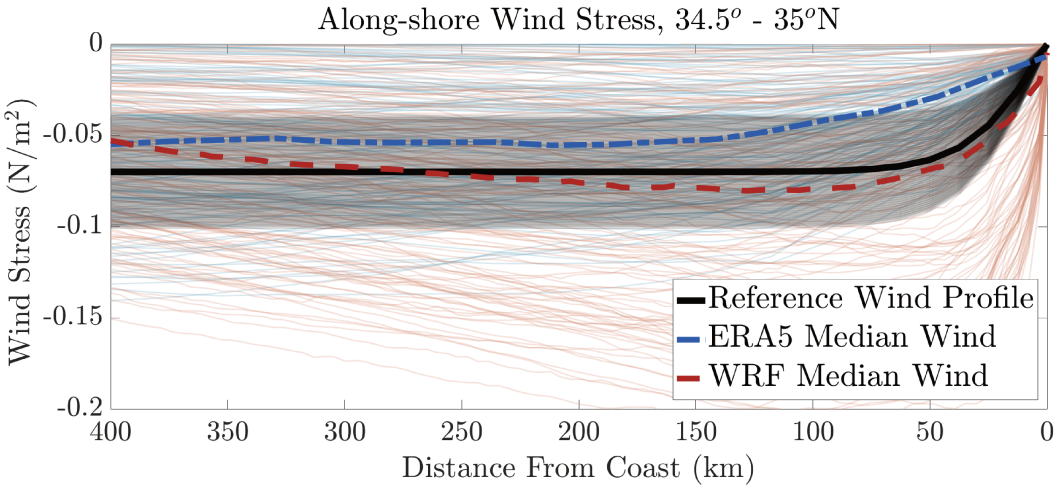

Figure 2: Wind profiles derived from ECMWF Reanalysis v5 (ERA5), and Weather Research & Forecasting Model (WRF), in blue and red, respectively. The thick lines show the median wind profiles for each reanalysis product, and the black line shows the reference wind profile used in MAMEBUS, with the black shaded area indicating the range of profiles used in the sensitivity analysis. The thin lines correspond to monthly averaged wind profiles from 1997-2017.

sion in size space, which allows for plankton to grow or shrink over relatively long timescales (Sauterey et al., 2017).

When size structured ecosystem models are highly resolved in trait-space and use size-dependent grazing interactions, the biomass aggregates along preferential modes, or peaks, along the size spectrum – a behavior that we refer to as size "quantization" (Banas, 2011; Moscoso et al., 2022). In zero dimensions, Moscoso et al. (2022) found that the location of these biomass peaks is approximately explained by a measure of selectivity in zooplankton grazing, namely, the width of the grazing profile, $\Delta\ell$. This variable controls the grazing behaviour of zooplankton with small values of $\Delta\ell$ limiting the number of size classes zooplankton can graze, and larger values allowing for less selective grazing. As such, small values of $\Delta\ell$ correspond to an ecosystem with highly specialized zooplankton grazers. In this configuration, there are more biomass peaks along the size spectrum with more plankton diversity in size space (Vallina et al., 2014). In the limit of $\Delta\ell \to 0$, there is no quantization in biomass (Poulin & Franks, 2010). While the formulation of the grazing controls the biomass peaks, the nutrient availability allows for the emergence of large size classes with the approximate spacing between peaks determined by the value of $\Delta\ell$. Quantization establishes on the timescale of approximately one year under both constant (Moscoso et al., 2022) and variable nutrient forcing (Banas, 2011).

The configuration of the model is similar to that presented in Moscoso et al. (2022), with the following changes: In this study, we set $\Delta\ell = 0.2$ as our representative grazing profile width (Hansen et al., 1994). Based on prior simulations, we use 50 phytoplankton and zooplankton size classes, as this is the minimal number of classes to resolve quantization in biomass and converge to a steady state equilibrium over time. The 50 phytoplankton size classes are log-linearly spaced between 0.2 μm and 100 μm, and the 50 zooplankton size classes are log-linearly spaced between 0.5μm and 5000μm. All phytoplankton classes are initialized to a constant value of 0.1 mmol N m^{-3}, and all zooplankton are initialized to 0.01 mmol N m^{-3}.

We simulate a single nutrient pool that represents nitrate, since nitrogen is the main limiting nutrient in the California Current (Deutsch et al., 2021), and nitrate fluxes are often used in EBUSs as proxies of productivity (Chavez & Messié, 2009; Messié et al., 2009; M. Jacox & Edwards, 2012). Note that the model formulation does not explicitly include a distinction between new and regenerated production (Karl, 2002). However, in regions of high productivity, new production often dominates over regenerated production (Sarmiento & Gruber, 2006; Messié et al., 2009). The nitrate profile is initialized to the restoring profile everywhere in the domain, but only restored in the sponge layer after initialization, as described by Equation 3.

The model includes a single particulate detritus pool, with a constant sinking speed of 10 m d^{-1}. Thus, we do not include size-dependent sinking or size structure in the detritus component, recognizing that this choice may be important in determining vertical nutrient fluxes to the deep ocean (Kriest, 2002; Polimene et al., 2017). Detritus is initialized to zero everywhere in the domain and at the lower boundary detritus has a no flux condition, and is remineralized to nitrate in the lowest grid-cell.

At the western boundary, nitrate is restored to an idealized profile defined as,

$$N_R(z) = \begin{cases} 0 & z \leq \zeta_N^0 \\ N_{\min} - N_{\max} \tanh\left(\frac{z+\zeta_N^0}{\Delta\zeta_N}\right) & z > \zeta_N^0 \end{cases} \tag{3}$$

where $N_{\min}$ is the minimum surface nutrient concentration, $N_{\max}$ is the maximum subsurface nutrient concentration, ζ_N^0 is the nutrient restoring depth, and $\Delta\zeta_N$ is the nutrient decay scale. This functional representation is based on an idealized fit to observations, shown in Figure 3, with parameters tuned to approximately track the median profile of all observations. Note that both the thermocline and nutricline do not always align in the data (not shown) and are characterized by variable vertical scales. Thus, the profiles of these two variables are varied independently in the parameter sweeps presented in Section 2.3.

2.3 Sensitivity Experiments

The parameter range for the wind profile and nutrient restoring profile are chosen from data and reanalysis products, with perturbations that represents natural variability in the data. The ranges of the eddy diffusivities are informed by previous work by Colas et al. (2013), Abernathey & Marshall (2013) and Swenson & Niiler (1996). For each of parameter configuration, the model is spun-up with physics only for 30 model years with constant wind forcing, and buoyancy restoring at the surface and in the western sponge layer. For computational efficiency, the biogeochemical component of the model is activated during the last 10 model years (corresponding to a total of 40 years of physical integration, and 10 years of coupled model integration). During the biogeochemical spin-up, the size-structured ecosystem model exhibits some internal variability in the location of the biomass peaks. However, the peaks are well established after 1 model year, and sharpen over the remainder of the model run in both 0D and 1D configurations (Moscoso et al., 2022). The biological model is considered spun-up when the L2 norm of the difference in biomass for every size class between time-steps is small ($O(10^{-3})$ mmol N m^{-3}), for the reference state. This occurs after approximately five years, but the model is run for twice that length for analysis. All data reported and visualized in this study is averaged over the final model year. The range spanned by each parameter is shown in Table 1.

2.3.1 Wind Stress Forcing, τ_{max} and τ_x

The two parameter sweeps that we choose to control the wind-profile are $\tau_{\max}$, the maximum offshore wind stress, and τ_x, a tuning parameter that allows us to control the width of the wind stress curl. The ranges of values for $\tau_{\max}$ and τ_x are shown in Table

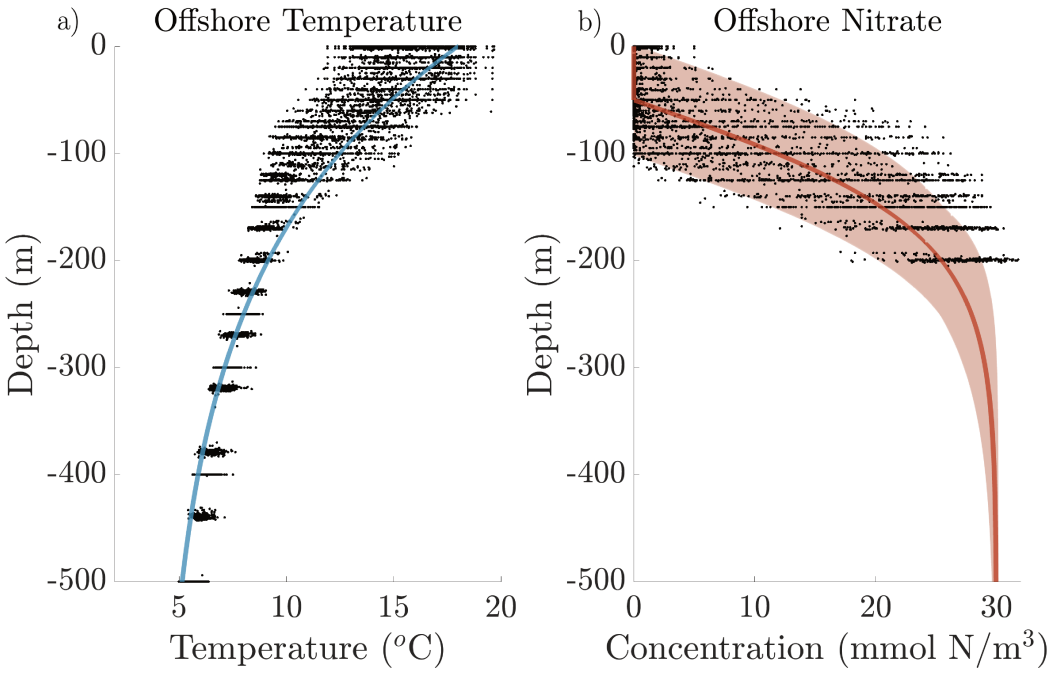

Figure 3: Restoring profiles for the temperature (left) and the nitrate (right). The black dots show data taken along Line 80 at stations 90 and 100 from California Cooperative Oceanic Fisheries Investigations (CalCOFI). Each point represents a nitrate measurement taken during cruises conducted in January, April, July, and October between 1997 and 2018. The shaded area (b) indicates the range of profiles used in the sensitivity analysis.

Table 1: Parameters varied in this study.

Parameter	Reference Value	Perturbation Range	Data or Reference	Description
$\tau_{\max}$	0.05 N/m^2	[0.01,0.1] N/m^2	ERA5 and WRF Castelao & Luo (2018)	Offshore wind stress maximum
τ_x	12	[4, 18]	ERA5 and WRF Albert et al. (2010)	Width of wind stress curl
ζ_N^0	50 m	[0,100] m	CalCOFI	Nutrient restoring depth
$\Delta\zeta_N$	120 m	[80,160] m	CalCOFI	Nutrient decay scale
κ_{GM}	1200 m^2/s	[600, 1600] m^2/s	Swenson & Niiler (1996)	Maximum surface buoyancy diffusivity
κ_{iso}	2400 m^2/s	[1600, 2400] m^2/s	Abernathey & Marshall (2013)	Maximum surface isopycnal diffusivity

1, and are chosen to span the range of data from ERA5 and WRF. M. Jacox & Edwards (2012) find that a nearshore reduction in wind stress reduces inner shelf circulation and bottom boundary layer transport in the region of the wind stress curl. As a result, wind stress profiles with substantial nearshore curl show stronger upwelling and nutrient injection into the surface layer, while wind stress profiles with weaker near-shore curl show reduced surface nutrient concentrations (Albert et al., 2010).

2.3.2 Eddies, κ_{GM} and κ_{iso}

There are two components to the eddy parameterization in MAMEBUS that may have distinct impacts on ecosystem diversity: eddy advection (Gent & McWilliams, 1990),

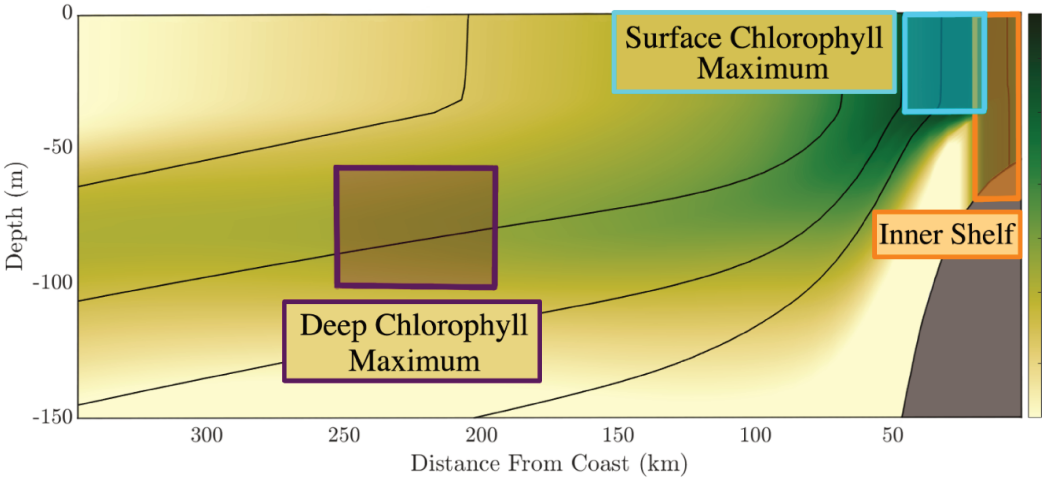

Figure 4: A schematic of the locations where ecosystem metrics are calculated. Metrics defined on the inner shelf are area averaged over the region where the surface and bottom mixed layers overlap. The surface chlorophyll maximum is defined as 25 km around the horizontal center of phytoplankton mass averaged over the mixed layer. The deep chlorophyll maximum is defined as the vertical center of mass of the total phytoplankton concentration averaged over 200-250 km from the coast, and 50 meters vertically. Color shading shows an example of phytoplankton distribution in the model, with temperature contours.

and isopycnal mixing (Redi, 1982). In these two parameter sweeps, we vary the strengths of the buoyancy diffusivity κ_{GM}, and the isopycnal diffusivity κ_{iso}. Reference profiles of the buoyancy and isopycnal diffusivity are shown in Moscoso et al. (2021) with surface intensified mixing (Lacasce, 2017). Additionally the reference values and the parameter variations of κ_{GM} and κ_{iso} are given in Table 1.

2.3.3 Offshore nutrient profile (boundary conditions), ζ_N^0 and $\Delta\zeta_N$

In MAMEBUS, two parameters control the nutrients profiles in the open ocean. The first is the nutrient restoring depth, ζ_N^0. This parameter allows us to set the level of oligotrophy in the surface ocean. Figure 3 shows the variations of the nutrient profile between 1997 – 2018 from Line 80 in CalCOFI. The nutrient restoring depth ζ_N^0, varies from zero nutrients at the surface, to zero nutrients up to 100m depth. The second is the nutrient decay scale with depth, $\Delta\zeta_N$, which we vary to span the variability found in measured nutrient concentrations. The reference values and parameter variations of ζ_N^0 and $\Delta\zeta_N$ are given in Table 1.

2.4 Model Diagnostics

In this section, we define sub-regions in the model domain that are important to productivity in EBUSs and model diagnostics that will be calculated in each of these regions. The sub-regions we identify are the shelf, the surface chlorophyll maximum (SCM), and the deep chlorophyll maximum (DCM).

2.4.1 Inner Shelf

The inner shelf area is defined as the region on the shelf where the surface and bottom mixed layers overlap, shown in orange on Figure 4. This region is chosen because

Table 2: Table showing the area averaged model diagnostics calculated in the surface chlorophyll maximum, on the shelf, and in the deep chlorophyll maximum.

Diagnostic	Description
$X^{\text{surf}}_{\text{max}}$	Surface Chlorophyll Maximum location
ζ_{DCM}	Deep Chlorophyll Maximum location
P_{tot}	Total phytoplankton concentration
Z_{tot}	Total zooplankton concentration
T	Temperature
U	Total uptake of nutrients by phytoplankton
ℓ^*_p	Concentration-weighted average size
H	Shannon index

upwelling is confined to the bottom boundary layer which directly links the surface to the subsurface. In all of our model simulations, the mixed layers overlap at approximately 25km from the coast. In this study, we do not vary the depth of the mixed layers, however, changes in mixed layer depths may be important in determining the nearshore concentration of plankton. The location of the inner shelf in the reference solution is shown in the orange box in Figure 4. Generally, the inner shelf is considered to be the shoaling region that connects the surf-zone to the continental shelf (Lentz & Fewings, 2012). However, we do not resolve a myraid of dynamics that are indicative of the inner shelf, including tides, buoyant plumes, and waves. For simplicity, we refer to the inner shelf region in this paper as the "shelf".

2.4.2 Surface Chlorophyll Maximum (SCM)

We identify the surface chlorophyll maximum (SCM). Often in the CCS, we observe a coastal surface maximum in chlorophyll nearshore. However, this region may not occur over the shelf and can extend over the slope, as described in Section 2.4.1 because it may be closely tied to the ventilation of subsurface nutrients. We define the location of the SCM as a concentration-weighted distance from the coast, averaged vertically over the surface mixed layer, ζ_{sml}. Mathematically, we define the SCM as,

$$X^{\text{surf}}_{\text{max}} = \frac{1}{P^A_{\text{tot}}} \overline{\int (P_{\text{tot}} \cdot x)\, \mathrm{d}x}^{\,\zeta_{\text{sml}}}, \tag{4}$$

where P^A_{tot} is the total phytoplankton concentration in the integrated area, and P_{tot} is the total plankton concentration in the center of each model grid-box. An example of the location of the surface chlorophyll max is shown in the blue box in Figure 4.

2.4.3 Deep chlorophyll maximum (DCM)

DCMs are a common feature in EBUSs. The depth of the DCM is dependent on the balance between light available in the water column and nutrients available below, in regions where nutrients are not entrained into the surface mixed layer (Cullen, 1982; Zubkov et al., 2000; Tréguer et al., 2018). Brandini et al. (2014) proposed that a component of the horizontal advection could bring nutrients and productivity into the DCM from regions of strong Ekman forcing, but the magnitude of this contribution is not well constrained.

The DCM is defined as the off-slope region of the domain beneath the surface mixed layer, ζ_{sml} and above $\zeta_e = 200$ m depth, to encompass the depth of the euphotic zone.

This location of the DCM in the model domain is calculated halfway between the Eastern and Western boundaries of the domain. This choice was made to include the theoretical maximum depth of the euphotic zone, ~ -115 m in the absence of plankton and detrius, given our formulation of the irradiance profile in the biogeochemical model. The depth of the DCM is calculated as a biomass-weighted average depth,

$$\zeta_{\mathrm{DCM}} = \frac{1}{P_{\mathrm{tot}}} \overline{\int_{\zeta_e}^{\zeta_{\mathrm{sml}}} (P \cdot z)\, \mathrm{d}z}^{\,x} \quad . \tag{5}$$

2.4.4 Ecosystem metrics

We introduce a series of metrics to quantify how ecological diversity responds to a set of physical forcings. The first is the concentration-weighted average size, defined as

$$\ell_p^* = \frac{1}{P_{tot}} \sum_i^{n_p} P_i \ell_{p_i}, \tag{6}$$

where P_i is the concentration of phytoplankton in the i-th size class, $P_{tot} = \sum_i P_i$, is the total phytoplankton concentration, $\ell_{p_i} \log_{10}(\mu\mathrm{m})$ is the size of the phytoplankton in the i-th size class in log-space, and n_p is the number of phytoplankton size classes. If ℓ_{p^*} is large the center of planktonic mass in a specific model region is shifted toward larger phytoplankton size classes. Similarly, smaller average size indicates that the biomass is concentrated in smaller planktonic size classes.

To characterize the diversity of the planktonic ecosystem, following Spellerberg & Fedor (2003), we define the Shannon Index, H as,

$$H = -\sum_{i=1}^{n_p} \frac{P_i}{P_{tot}} \ln\left(\frac{P_i}{P_{tot}}\right). \tag{7}$$

We use the Shannon index to quantify the size diversity in various model regions. Formally, the Shannon index is a measure of evenness in ecology, with lower values indicating that biomass is more evenly distributed across all size classes. Together, the average size and the Shannon Index allow us to identify, for example, regions of the model domain with the bulk of the phytoplankton biomass concentrated in the largest size classes (i.e. large ℓ_{p^*} and H).

We also include area-averaged diagnostics of total phytoplankton concentration, $\overline{P}$, total zooplankton concentration $\overline{Z}$, temperature $\overline{T}$, and the total uptake of nutrients by phytoplankton $\overline{U}$, a measure of net primary production. Here, the overbars denote area averages over the different diagnostic regions. The representation of uptake is described in Moscoso et al. (2022).

3 Simulated state and ecosystem properties

The model reproduces general patterns of productivity characteristic of EBUSs and the CCS including high productivity nearshore, a transition zone offshore, and a subsurface DCM (Figure 5). At the surface, the model captures the zonal pattern of high biomass at the surface near the coast, and low biomass offshore. Similar patterns exist in zooplankton concentration. The DCM occurs at approximately 67m deep between 200-250 km from the coast.

The plankton biomass is concentrated around several specific locations along the size spectrum, exhibiting quantized behavior. Moscoso et al. (2022) conclude that biomass quantization is controlled by grazing, with the emergence of large size classes at increasingly high nutrient supply (Armstrong, 1994) and a gap between biomass peaks matching well theoretical estimates. Near the coast, where the total biomass is the highest, the

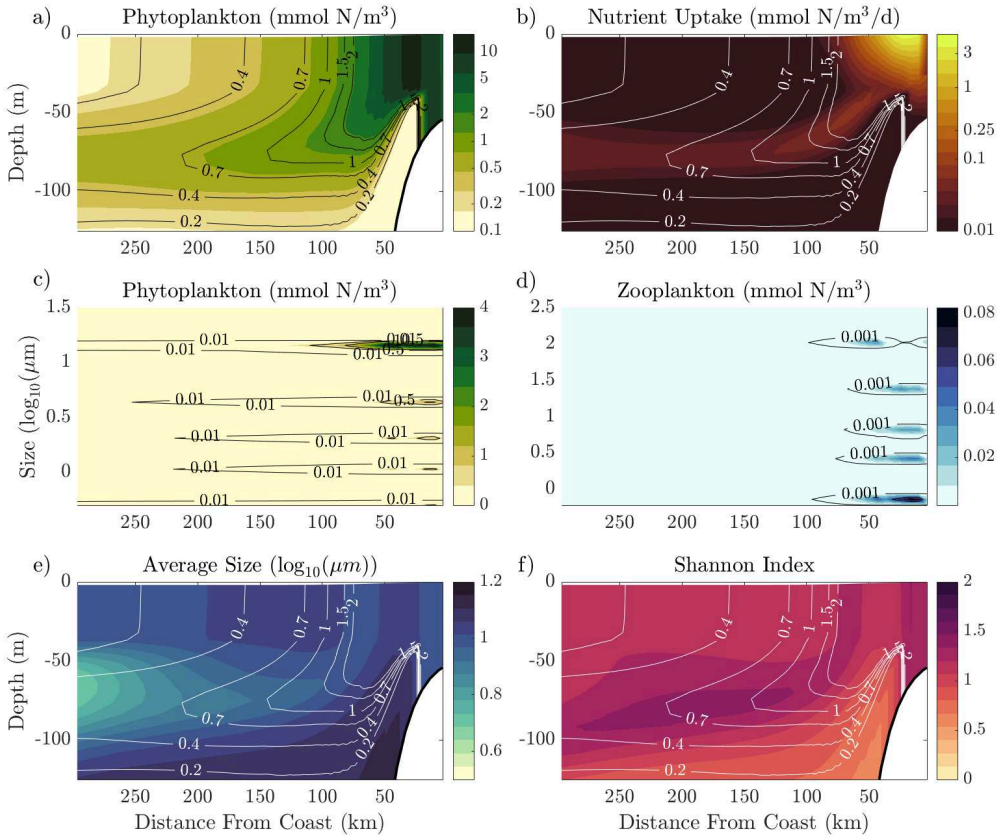

Figure 5: Size structure in our reference simulation over the model domain, outside of the restoring sponge layer at the western boundary. The top row of panels show the (a) total biomass of phytoplankton, and (b) the nutrient uptake per day. In (a) and (b), the total concentration of phytoplankton is shown in black and white contours, respectively. The middle panels show the biomass of (c) phytoplankton, and (d) zooplankton, averaged in the surface mixed layer as a function of distance from the coast and plankton size. The black lines in (c) and (d) are the biomass contours. The bottom panels show ecosystem metrics that consist of (e) concentration-weighted average size, and (f) Shannon Index. In (e) and (f), the total concentration of phytoplankton is shown in white contours.

largest phytoplankton size class contributes most to the total biomass. Offshore, the large size class still persists; however the intermediate size classes are not present above a concentration of 0.01 mmol N m^{-3}. At depth across the entire domain, the average size of phytoplankton skews high, but the total biomass remains small. In this region, the largest size class does persist at very low concentrations. This regular spacing breaks down at approximately 170 km from the coast, where the width between peaks begins to increase. Here, the largest and smallest phytoplankton size classes persist. We assume that mortality is linearly proportional to phytoplankton uptake (n.b. Banas (2011)), therefore at small nutrient concentration, and thus slow nutrient uptake at large phytoplankton size classes, larger phytoplankton mortality is reduced. In regions, such as the surface mixed layer, with strong Ekman transport, large phytoplankton size classes may persist offshore.

Qualitatively, we find that large phytoplankton contribute to most of the biomass on the shelf. This is supported by a variety of observations, e.g., Hood et al. (1991) who found that large phytoplankton dominate at the surface in the shoreward side of an upwelling front. Offshore, in regions with lower total concentration, smaller phytoplank-

ton persist across more of the domain than the middle size classes. Figure 5 shows that the intermediate size classes are present in the nearest 200-250 km from the coast above 0.01 mmol m−3. Previous work (e.g., Worden et al. (2004) and Taylor et al. (2012)) also shows that small phytoplankton dominate in the subtropical gyre and away from the nutrient-rich regions of the upwelling front.

Similar to phytoplankton, zooplankton also exhibit quantization. However, most of the biomass is concentrated in the smallest size classes in the surface waters within 100km from the coast. We suspect that this is a consequence of faster grazing rates for smaller zooplankton, faster mortality, and a wide grazing profile. In reality, we would expect the smaller zooplankton size classes to persist further offshore; however, here, zooplankton are mostly found on the shelf. Away from the coast, offshore of 100km, are very small concentration of zooplankton, < 0.001 mmol m−3, which may explain the dominance of large phytoplankton offshore.

Figure 5 shows measures of the average size, ℓ_p, and the Shannon Index, H, for phytoplankton over the model domain in the mixed layer. Near the coast, in regions with high nutrient concentration and plankton biomass, the average size is the largest. Beneath the surface mixed layer, ($Z < -30$ m), the average size decreases, and in the DCM the smaller sizes dominate. For large values of H, the biomass is more equally distributed over many size classes, and for smaller values of H the biomass is aggregated among many size classes. In the SCM, the Shannon index slightly decreases, as the largest phytoplankton size class dominates in total biomass. Offshore and in the subsurface, the biomass is more evenly distributed, which is reflected in the Shannon Index. Between 50 and 100 m depth, approximately 300-350 km offshore, where the average size is at a local minimum, the Shannon index slightly decreases, implying that the smallest phytoplankton size classes dominate in this region. Below 125m depth, for total phytoplankton less than 0.2 mmol N m^{-3}, the largest size class persists, and dominates the total biomass.

A model-data comparison is additionally included in the Supplementary Information (see Figure S20 and associated text).

4 Ecosystem Sensitivity

In this section, we present the simulated responses of the model's physical state and ecosystem structure to variations in our control parameters (see Section 2). To quantify the model sensitivities, we normalize each diagnostic by its corresponding value from our reference simulation. In the same vein, the value of each control parameter, p, is normalized by the corresponding reference value, p_0, in Table 1. This normalization allows us to compare relative changes with respect to reference values for all parameters and diagnostics simultaneously. With this normalization, we conduct linear fits for each of the parameter sweeps and use the slope of the best fit to identify the most important control parameters. Additionally, we calculate the percentage of variance about the best fit line, i.e., the R^2, to determine how well a linear relationship explains the model behavior. Figure 6 shows the diagnostics (listed in Table 2) and the associated best fit line. The reference values for each of the control parameters in the diagnostic regions is listed in Table S1 in the Supplementary Information. Additionally, a full set of figures for each diagnostic is shown in the Supplementary Information .

While linear relationships are often useful in determining the first order behavior between our control parameters and model diagnostics, in some cases, a non-linear could be a more appropriate. To consider these cases, we calculate a secondary measure of of best fit with a second degree polynomial increases the measure of best fit. We list the leading coefficient, the R^2 value for the quadratic fit, and the difference between the measures of best fit for the polynomial and linear fits, see Figure S19 and Tables S2-S4. In general, an additional degree including an additional degree of freedom allows for a bet-

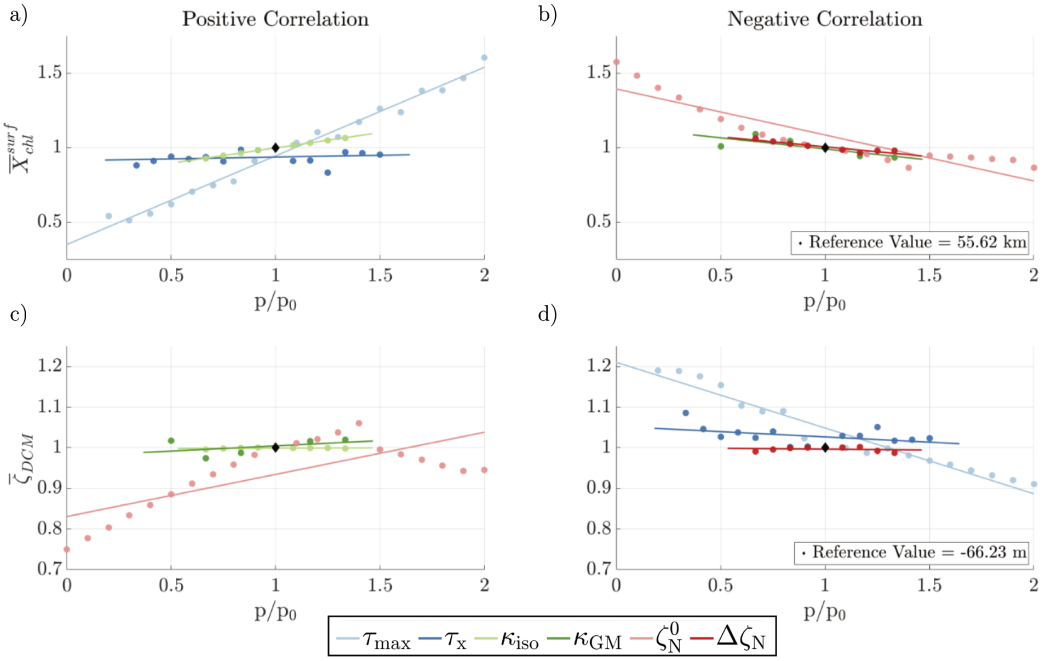

Figure 6: Responses of the location of the surface chlorophyll maximum (a,b) and the depth of the deep chlorophyll maximum (c,d). Model diagnostics are normalized relative to values from the control solution. Parameter sweeps with positive correlations are shown in the left column (a,c) and negative correlations in the right column (b,d). Parameters are normalized relative to the reference values (p_0) for comparison across parameter sweeps where τ_{max} is the maximum wind-stress, τ_x is the width of the wind-stress curl, κ_{iso} is the isopycnal mixing coefficient, κ_{GM} is the eddy advection coefficient, ζ_N^0 is the nutrient restoring depth, and $\Delta\zeta_N$ is the width of the nutricline.

ter fit, therefore we select a threshold to indicate non-linear responses to the variables in our control parameters as $(R^2_{\text{quad}} - R^2_{\text{lin}}) > 0.25$. In other words, 25% more of the variance is explained using the quadratic model.

We focus first on the sensitivity of the SCM and DCM positions, and then on the ecosystem response at these location to wind, eddies, and boundary conditions. We also identify significant correlations between various model diagnostics (Figure 8).

4.1 Regions of model diagnostics

In the reference case, the SCM is located approximately ~ 56 km from the eastern boundary of the model domain. The magnitude of the offshore wind-stress maximum is strongly correlated with the location of the SCM, with an increase in wind-stress increasing $\overline{X}^{\text{surf}}_{\text{chl}}$ (Figure 6 and 8). For brevity in this section, the values of the slopes and corresponding measures of best fit, R^2, are given in the Supplementary Material. Dynamically, the strength of the wind determines the mean upwelling transport that carries nutrients to the surface (M. J. Jacox & Edwards, 2011; Capet et al., 2004; Bakun & Nelson, 1991), so this result agrees with previous findings. The location of the SCM is also sensitive to the nutrient restoring depth, ζ_N^0. A shoaling of the nutrient restoring depth pushes the front offshore – i.e., it expands the productive coastal region. Likewise, a deepening moves the location of the SCM shore-ward, although with a weaker sensitivity. This response likely reflects total nutrient concentration in the source wa-

ters that are upwelled onto the shelf (M. J. Jacox & Edwards, 2011). In this case, we assume that the nutrient flux is a function of the upwelling flux and nutrient concentration, so the total upwelling and the nutrient concentration at upwelling depth are relevant.

The depth of the DCM, with a reference value of ~ -66m, is less sensitive to changes in physical drivers. There is some dependence on the nutrient restoring depth, and the offshore wind-stress maximum. An increase in the magnitude of the wind-stress is associated with a shoaling of the DCM, and a strongly linear response (R^2=0.94). With increasing wind-stress, the strength of the upwelling increases, and more nutrients are brought to the surface (Capet et al., 2004; Messié et al., 2009). This shoals the nutricline in the model domain, driving the DCM toward the surface. Previous studies have proposed that the depth of the DCM is determined by a balance between the available light that penetrates from the surface and the nutrient availability at depth (Cullen, 1982; Zubkov et al., 2000; Tréguer et al., 2018). Nutrient profiles in turn are affected not only by lateral and vertical advection, but also by redistribution of organic matter by sinking particle fluxes, and subsequent remineralization. In this perturbation experiment, the depth of the DCM deepens with the nutrient restoring depth, although with very deep restoring depth, this relationship exhibits some nonlinearity. Light penetration from the surface is an important control on the depth of the DCM, and at very deep restoring there may be a compensation between the nutrient distribution and light limitation. In fact, we see that the phytoplankton biomass substantially decreases as nutrient restoring depth deepens.

The depth of the DCM exhibits non-linearity in the response to perturbations in ζ_N^0. There is a domed shape in overall response to the depth of the nutricline. Over our parameter sweep, the depth of the DCM reaches a maximum at $1.4p/p_0$, and shoals, due to a combination of light and nutrient limitation.

4.2 Wind

Nearly all model diagnostics show a positive sensitivity to the wind stress maximum. Stronger winds increase the concentrations in phytoplankton and zooplankton across the model domain. The uptake on the shelf shows the strongest sensitivity, although the total biomass does not change as dramatically. Diagnostics of ecosystem diversity, ℓ_p and H, show small positive slopes and small R^2 values, indicating weak, nonlinear sensitivities (Figures S3 and S4). At very strong wind stress, the average size decreases due to the emergence of a new size class as a consequence of increased nutrients at the surface and in the SCM (see Figures S7 and S13). Similar nonlinear behavior is further seen in the DCM (see Figure S16 and S19). This can further be confirmed by a negative correlation in the shelf temperature, which implies stronger upwelling near the coast (Capet et al., 2004).

The width of the wind-stress curl has a significant negative impact on the zooplankton biomass in the DCM, while showing a minimal effect on phytoplankton biomass. This impact on zooplankton may reflect a negative impact on phytoplankton uptake. Further, the average size in the DCM increases when the width of the wind-stress curl decreases (Figure S6, and S16). However, this pattern is nonlinear with a peak near in the middle of our parameter space. A possible explanation for this could be that at low wind-stress forcing, an increase to upwelling allows for more nutrients to be delivered to the DCM. At high levels of forcing, a possible explanation could be that an increase in eddy activity and further remove nutrients from the DCM limiting large phytoplankton growth. The response is nearly opposite on the shelf, where a sharper wind-stress curl increases uptake and zooplankton biomass, while uptake slightly decreases in the SCM. This may indicate some non-linearity in the solutions, for example, see Figure S1 and S19.

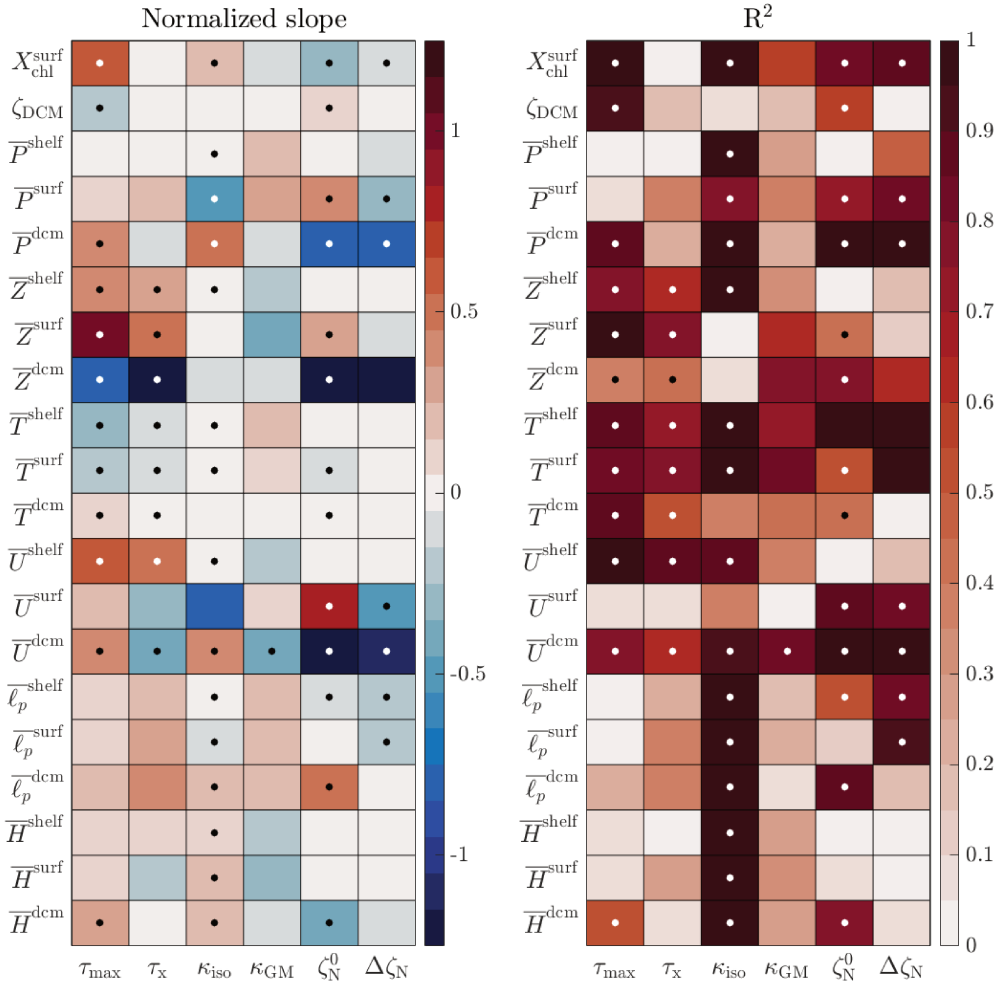

Figure 7: Correlation matrix showing the slope of the best fit line for each diagnostic (rows) along with the measure of best fit or R^2 value. The slope of the best fit line for each metric as a function of the control parameters (columns) is shown on the left. Each metric is area-averaged on the shelf, in the surface chlorophyll maximum, and in the deep chlorophyll maximum over one model year. The bullets in the center of the boxes indicate correlations that are statistically significant using the linear Pearson's correlation ($p < 0.01$).

Specific non-linear behavior can be seen in the average size of phytoplankton in all three diagnostic regions, in the phytoplankton biomass and the diversity index in the SCM and on the shelf, see Figure S19. Combined, this behavior indicates that there is an optimal wind-stress which allows for a local maxima in the phytoplankton biomass and size, with a reduction in productivity at high wind-stress. This result follows work presented by Botsford et al. (2006) and García-Reyes et al. (2014).

4.3 Eddies

The isopycnal diffusivity, κ_{iso} shows statistically significant relationships with plankton biomass in all the diagnostic regions. The total phytoplankton biomass in the SCM and DCM show strong negative and positive slopes, respectively. This suggests that κ_{iso} transfers nutrients and phytoplankton from the SCM to the DCM. Our results are con-

sistent with previous work by Gruber et al. (2011), which showed that eddies tend to sequester nutrients to depth and decrease surface productivity. While we find statistically significant relationships between the average phytoplankton size and the Shannon Index in the diagnostic regions, these relationships are weak (see Figures S9). In the SCM, higher isopycnal diffusion slightly decreases the average size of phytoplankton, while increasing the Shannon Index. Similar patterns are observed on the shelf (Figure S14). In both regions, the slight increase in diversity likely corresponds to a reduction of biomass in the larger size classes. Finally, in the DCM, both average size and diversity increase, likely as a result of increased nutrient supply by eddy stirring along isopycnals (Figure S17).

The effect of eddy restratification κ_{GM} is relatively small. On the shelf and in the SCM, increasing κ_{GM} causes an increase of the total phytoplankton, but a decrease of total zooplankton. The average size of the phytoplankton increases, and the Shannon index decreases, implying that the biomass shifts toward larger sizes. However, the only statistically significant correlation is for the average uptake in the DCM; with increasing κ_{GM}, the total uptake in the DCM decreases as the surface ocean gets more stratified. Overall, the slopes of most of the relationships are small, with low R^2 values.

Figures provided in the Supplementary information show substantial variability about the best fit line, suggesting nonlinear responses to changes in the eddy fluxes (see Figures S10, S14, S17, S19). Quadratic fits can better explain the behavior in the average phytoplankton size across the domain with respect to κ_{GM}. There is also a slight decrease in the variance in the total biomass in the DCM and on the shelf, with diagnostics showing a local maximum in the domain, with non-negligible leading coefficients (see Figure S19). This indicates that there is a local maximum in the the size and biomass as κ_{GM} increases. A possible explanation for this could be that at low κ_{GM}, increasing the effect of restratification increases the transport subsurface. However, with sufficient upwelling, this allows for the size and biomass to continue to increase. At high values of κ_{GM}, large stratification inhibits deep upwelling, decreasing the upwelled nutrient concentration, total biomass in the surface and thus average phytoplankton size.

4.4 Offshore nutrient profiles

The nutrient restoring depth has strong impacts on the ecosystem behavior in the DCM. The total biomass of plankton in the DCM has strong, statistically significant negative slope, implying that as the nutrient restoring depth deepens, the phytoplankton concentration decreases (see Figures 7 and S5). Additionally, the average size increases in the DCM, and the Shannon index decreases, implying that larger sizes out-compete smaller sizes in this region (see Figure S18). In the ecosystem model, we impose limits on minimum phytoplankton biomass. Thus the skew toward larger sizes may be explained by a combination of horizontal advection of large cells into the DCM and slow mortality rates. The decrease in average uptake also supports this conclusion, as larger sizes have slower uptake rates. However, this phenomenon in our model requires further investigation. On the shelf, the relationship between the nutrient restoring depth and temperature is statistically significant, with positive slopes implying that, as the nutricline deepens offshore, more plankton biomass remains at the surface as large phytoplankton out compete smaller phytoplankton (see Figure S15). The average size has a slightly negative correlation, implying that the phytoplankton at the surface are overall smaller as the nutricline deepens as a consequence of reduced nutrient availability (see Figures S11 and S12). A possible explanation for this could be that the source depth of upwelled waters is deep enough to provide a sufficient source of nitrate to the surface.

The nutrient decay scale, which approximates the thickness of the nutricline, reduces total plankton biomass in the DCM. However, the average size and the Shannon index in the DCM are not as sensitive to this parameter (Figure S18). In the SCM, the

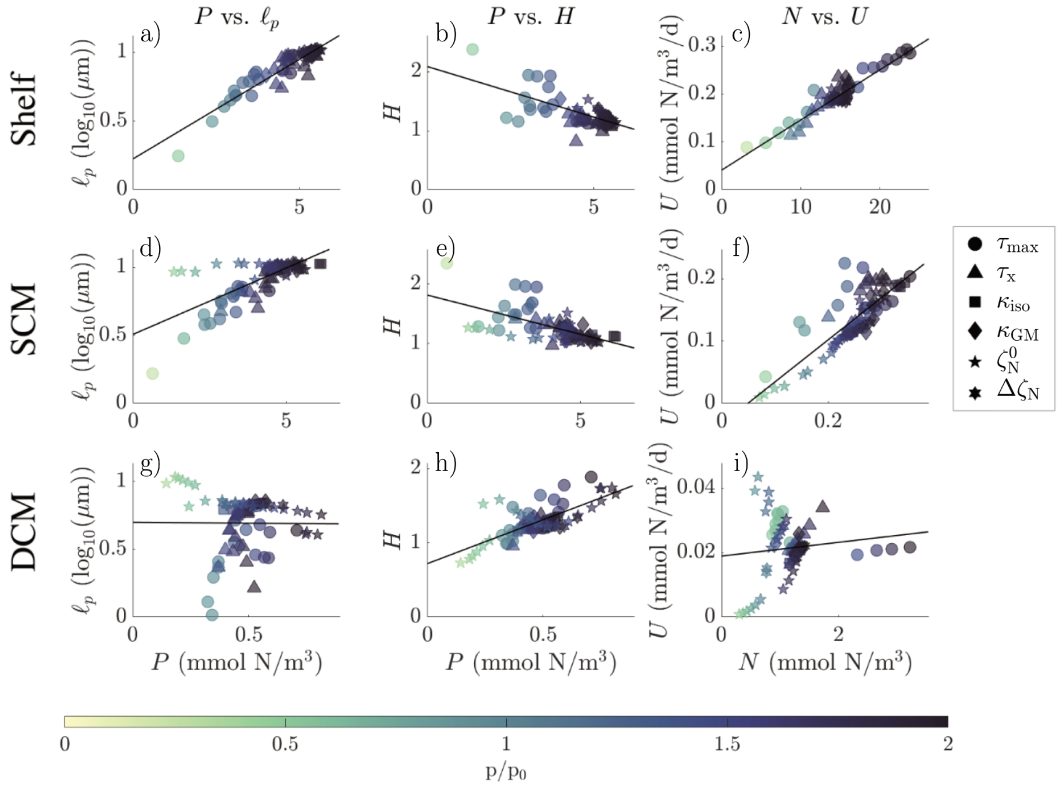

Figure 8: Relationships between measured concentrations of phytoplankton and size (a,d,g), phytoplankton biomass and Shannon Index (b,e,h), and nitrate and uptake by phytoplankton (c,f,i). These relationships are calculated on the shelf (a,b,c), the surface chlorophyll maximum (d,e,f), and in the deep chlorophyll maximum (g,h,i) across the entire suite of simulations. Marker shapes correspond to different control parameters, as indicated in the legend. The color of the marker is associated with the normalized magnitude of the corresponding control parameter, with darker colors indicating the larger values.

total plankton concentration decreases, likely driven by a decrease in total concentration of nitrate in source waters. This trend is further supported by a decrease in the average uptake (see Figure S12). While the total phytoplankton and zooplankton concentration decreases, the size distribution does not change significantly, or slightly decrease. At the SCM, there is a statistically significant decrease in the total phytoplankton concentration and total uptake reflecting lower nutrient concentrations in the source waters. We also observe a statistically significant decrease in the average phytoplankton size on the shelf and at the surface (Figure S15). However, the trends in phytoplankton biomass and nutrient uptake are not statistically significant.

4.5 Controls on ecosystem composition

Figure 8 shows the correlations between model diagnostics in the surface, SCM, and DCM. This comparison allows us to identify likely controls on ecosystem composition with respect to nutrient concentration and phytoplankton biomass.

On the shelf, we observe a linear relationship between the total phytoplankton concentration and the average size across our parameter sweeps. This indicates that as to-

tal phytoplankton concentration increases, the average size also increases, in agreement with previous studies (Taylor et al., 2012; Worden et al., 2004; Van Oostende et al., 2018; Moscoso et al., 2022). Similarly, as the total nutrient concentration varies on the shelf, the total uptake shows a linear response, increasing with nutrient concentration across our parameter sweeps. The Shannon Index, however, decreases with increasing phytoplankton concentration. An increase in the average size, but a decrease in the Shannon Index indicate that the largest size class contributes most of the biomass on the shelf. The behavior is similar in the SCM. A major outlier occurs in the relationship between the total phytoplankton biomass and average size with respect to the nutrient restoring depth (see Figure 7). In the SCM, away from the region of strongest upwelling, the total nutrient concentration is much smaller than the shelf concentration; however, the phytoplankton biomass is approximately the same. This may be a consequence of Ekman transport in the surface mixed layer.

The total biomass and average size are not well correlated in the DCM. Similarly, the total nutrients and uptake are also not well correlated. A potential explanation for these responses is that the ecosystem composition in the DCM could be impacted by Ekman transport or horizontal advection from the shelf or SCM, which would bring larger plankton and nutrients into the domain. The nutrient restoring depth parameter is a major outlier in the relationship between average size and plankton biomass in the DCM. In this parameter sweep, as the nutrient restoring depth deepens, while the total phytoplankton concentration decreases, the average size increases (see Figure S6). A possible explanation here is that a combination of low mortality and slow grazing rates would benefit larger phytoplankton, driving the shift in both size and biomass.

Additionally, we observe a wide scatter in the relationship between total nutrients and uptake in the DCM. The outliers in this relationship are in model solutions with higher offshore wind-stress curl. While the total uptake with respect to the wind-stress do not show major outliers (see Figure S5), the total nutrient concentration seems to be the reason for the large deviation in the trends. This may be a result of the strong intensity of upwelling, which would bring more nutrients to the surface, with nutrient intrusions into the DCM in regions of stronger upwelling.

We observe a strong, positive relationship between the total phytoplankton concentration and the Shannon Index in the DCM, unlike in the SCM and on the shelf. Combining the relationships shown in Figure 8, this suggests that the Shannon index peaks when the phytoplankton concentration is approximately 1 mmol m^{-3}. In regions with lower phytoplankton biomass like the DCM, the average size is smaller than in the SCM and on the shelf (see Figure 5), with lower H, implying a few small size classes (Moscoso et al., 2022). As the total phytoplankton concentration increases, more size classes are able to emerge, expanding the diversity in the ecosystem. When the biomass increases above 1 mmol m^{-3} a larger proportion of the biomass is concentrated in the larger size classes, reducing diversity in the ecosystem.

5 Discussion

Strong productivity in EBUSs is driven by the upwelling of dense, nutrient rich water, which supports large phytoplankton blooms, and diverse ecosystems (Bakun & Nelson, 1991; Chavez & Messié, 2009). In regions of high productivity, large phytoplankton contribute to most of the biomass (Hood et al., 1991). In contrast, in regions of low productivity, smaller phytoplankton dominate (Zubkov et al., 2000; Worden et al., 2004). While previous studies have identified patterns of ecosystem productivity and size, it is unclear which physical parameters impact plankton diversity and size structure the most, and to what extent. In this study, we conduct a systematic sensitivity analysis to determine the important controls of ecosystem productivity and diversity in an idealized EBUS tuned after the California Current System. We show that the ecosystem responses

in three dynamically distinct regions: the inner shelf, the surface chlorophyll maximum, and the deep chlorophyll maximum. While we do not explicitly have formulations of scaling laws for these ecosystem metrics with respect to the parameter sweeps at this time, this study serves as a starting point. The purpose of this study is to investigate a subset of physical parameters that can control plankton diversity and size structure in EBUSs. The relationships identified in this study are thus ideally suited to allow formulation of mechanistic scaling laws that relate physical drivers to ecosystem characteristics in EBUSs.

We find that changes in the wind stress maximum and the nutrient decay scale have the largest impacts on planktonic biomass. Previous work has identified that the magnitude of the offshore wind stress is responsible for setting the total upwelling nutrient fluxes (Bakun & Nelson, 1991; Chavez & Messié, 2009; Messié et al., 2009; M. G. Jacox et al., 2014, 2018; Fiechter et al., 2018). Through all three diagnostic regions in our model, we find that the phytoplankton biomass increases with the wind stress maximum as a consequence of increased upwelling (measured by a decrease in temperature on on the shelf and in the SCM). On the shelf and in the SCM, phytoplankton show increasing uptake rates, but the total phytoplankton concentration exhibits saturating behavior, which can be explained by increased grazing by zooplankton (see Figures 7, and S3).

The offshore depth of the nutricline, ζ_N^0, shows a similar trend as phytoplankton biomass, with an increase in productivity in the SCM and a decrease in the DCM with deepening nutricline. The diagnostic regions of the model are sensitive to the nutricline depth, with the SCM moving shore-ward, and the DCM deepening with increasing nutricline depths. The decrease in plankton biomass in the DCM can be explained by a deepening DCM, which would limit light penetration from the surface, reducing productivity. The surprising response in this perturbation experiment is the increase in plankton biomass in the SCM. This trend may be explained by a shore-ward shift in the SCM, which would increase the total phytoplankton biomass as, $\overline{P}^{\text{surf}} < \overline{P}^{\text{shelf}}$, see Figures 7, S1, and S3. Chavez & Messié (2009) note that shoaling of the nutricline in EBUSs increases offshore surface productivity. This response in the model can be seen in the location of the SCM, which has a large offshore extent with very shallow nutricline depths, and in the DCM, which moves toward the surface.

Previous work indicates that a combination of eddy advection and along-isopycnal mixing are responsible for surface nutrient subduction (Gruber et al., 2011; Colas et al., 2013). The studies conducted by Gruber et al. (2011) and Colas et al. (2013) used an eddy resolving regional model of the CCS (Gruber et al., 2006), and the Peru-Chile System (Colas et al., 2012), with coupled eddy advective and diffusive fluxes. In our model, we are able to decouple these effects and study their consequences in isolation. Perhaps surprisingly, ecosystem properties appear very sensitive to perturbations in the isopycnal diffusivity, κ_{iso}. Variations in ecosystem properties with respect κ_{iso} show strongly linear relationships that are highly statistically significant. Previous work has shown that eddies remove nutrients and other tracers from the surface, and subduct them beneath the euphotic zone (Gruber et al., 2011; Kessouri et al., 2020). The quantities that more directly reflect this eddy-driven mechanism are the total concentration of phytoplankton, the total concentration of zooplankton, and the uptake of nutrients by phytoplankton. Increased eddy stirring reduces the phytoplankton and zooplankton concentration at the surface, and suppresses uptake of nutrients. In the DCM, on the other hand, there is an increase of phytoplankton and zooplankton, with increased uptake rates, which may reflect the eddy-driven supply of nutrients to the subsurface by subduction. The impact on the average plankton size and ecosystem diversity in the SCM and DCM, however, is minimal, suggesting that ecosystem diversity may be predominantly controlled by the grazing dynamics internal to the ecosystem (Vallina et al., 2014).

The impact of eddy advective fluxes, however, does not align with previous studies (Gruber et al., 2011; Colas et al., 2013). We find that variations in the buoyancy diffusivity, κ_{GM} in many cases have the opposite effect than the isopycnal diffusivity. For

example, the relationship between κ_{GM} and plankton biomass on the shelf has a local maxima within our parmater sweep, while the linear correlation of biomass at the surface is positive, while the correlation in the DCM is negative (see Figures 7, S1, S3, and S5). Thus, we suggest that eddy quenching is predominantly driven by eddy stirring along isopycnals.

With the exception of the wind stress maximum and the depth of the nutricline offshore, phytoplankton biomass between the SCM and DCM show nearly always opposite correlations. Phytoplankton biomass increases in the SCM and decreases in the DCM with narrower wind stress curl, a stronger eddy buoyancy diffusivity, and deeper nutriclines. The opposite behavior occurs with increasing isopycnal diffusivity. In the DCM, plankton biomass decreases; however, the potential mechanism for controlling this behavior has not been identified. Di Lorenzo (2003) and Rykaczewski & Checkley (2008) found that wider wind stress curl shoals isopycnal surfaces, which may impact the concentration of nutrients transported into the DCM. As a result, we may expect to see a shoaling of the DCM with smaller values of τ_x; however, the physical locations of the diagnostic regions remain largely unchanged. This disagreement with previous work may arise from the lack of momentum advection in the physical model formulation – an important driver of interior upwelling in the absence of an along-shore pressure gradient (Lentz & Chapman, 2004; Gruber et al., 2011; M. J. Jacox & Edwards, 2011; Connolly et al., 2014). These anti-correlated behaviors between the SCM and DCM across multiple parameters may point to connectivity between these two diagnostic regions, but the mechanisms that control this behavior require deeper investigation.

While many of the behaviors found in this study are well described by linear relationships there are trends that may be better described through non-linear fits. Given our idealized framework, many of the linear responses seen in this study may have more non-linear effects in more comprehensive regional modeling frameworks. Figure S19 indicates the behaviors which may be better described by non-linear behaviors. The control parameters that exhibit the most non-linearity in our framework are the wind-stress maximum (Botsford et al., 2006; García-Reyes et al., 2014; M. G. Jacox et al., 2016), the eddy restratification Gruber et al. (2011); Renault et al. (2016). Specifically, the average size and total biomass may be better understood in non-linear relationships in both the maximum wind-stress and the eddy restratification.

In our study, we focus on a small number of drivers that have been shown or suggested to affect the ecosystem behavior in EBUSs. However, additional controls may influence ecosystem diversity in these regions, and call for future work. For example, we do not include variation in the thickness of the surface and bottom mixed layers. Within the surface layer, phytoplankton are vertically mixed and exposed to a variety of light conditions as a consequence of light attenuation (Sverdrup, 1953; Huisman et al., 1999; Obata et al., 1996; Mahadevan et al., 2012), which may be important in determining the ecosystem composition, specifically nearshore where surface and bottom mixed layer merge. In the absence of along-shore pressure gradients, upwelling is mostly constrained to the bottom boundary layer (Lentz & Chapman, 2004; M. J. Jacox & Edwards, 2011). Previous studies have shown that the thickness of the bottom boundary layer increases in the presence of upwelling favorable winds, which likely impacts the nutrient availability on the shelf and in the SCM (Trowbridge & Lentz, 1998; Perlin et al., 2005).

We do not explore variations in topography. The continental slope has been shown to influence the strength of upwelling (M. Jacox & Edwards, 2012; Lentz & Chapman, 2004), and the depth of the shelf may be important in controlling the vertical exchange of nutrients with the bottom boundary layer (Perlin et al., 2005).

MAMEBUS has the ability to explore the effect of idealized along-shore circulation, but we did not explore this component of the model. However, this may be impor-

tant for the transport of subpolar or subtropical waters with different nutrient contents, and the delivery of nutrients to the subsurface by the poleward undercurrent.

While we focus predominantly on the lower trophic ecosystem, our findings have the potential to inform studies of food-web diversity (Andersen et al., 2016; Stock et al., 2017). In EBUSs and other productive regions, high productivity, dominated by large phytoplankton sizes, generally supports short, productive food-webs (Chavez & Messié, 2009) and rich fisheries (Ryther, 1969). Along with identifying potential controls on plankton diversity in EBUSs, we also show the persistence of biomass quantization in the presence of horizontal heterogeneity under a range of physical regimes. Similar to the findings presented in Banas (2011), Vallina et al. (2014), and Moscoso et al. (2022), while plankton productivity appears to be controlled by the nutrient availability, species diversity – here manifest as size quantization – is controlled by the specialization of grazing behavior. While we focus on the impact of biophysical parameters on phytoplankton size structure, Cheresh & Fiechter (2020) found that other important biological variables such as pH and oxygen are predominantly modulated by the strength of the wind and the composition of source waters.

The relationships between ecosystem properties shown in Figure 8 provide new insight into the responses of multiple metrics of ecosystem diversity and productivity to more regularly measured quantities (e.g. phytoplankton biomass and nutrient concentration). These findings may be extended and tested in realistic three-dimensional regional modeling efforts, and guide the development of theoretical scalings that have the potential to characterize productivity and ecosystem structure as a function of a wide set of physical controls.

Acknowledgments

The authors acknowledge resources from the Extreme Science and Engineering Discovery Environment (XSEDE, Towns et al., 2014), which is supported by National Science Foundation grant number ACI-1548562. J.E.M. and A.L.S. greatefully acknowledge support from the National Science Foundation through awards OCE-PRF #2205637 and OCE #1751386, respectively. D.B. acknowledges support from NOAA under Ecosystem and Harmful Algal Bloom (ECOHAB) Award NA18NOS4780174, and the Alfred P. Sloan Foundation. Without implying their endorsement, the authors would also like to thank Naomi Levine and Jim McWilliams for helpful conversations. The authors would also like to thank the anonymous reviewers for their helpful comments and suggestions which made the presentation of this study more clear.

Data Availability Statement: The DOI for the MAMEBUS code is https://doi.org/10.5281/zenodo.3866652 (Stewart and Moscoso, 2020). This package includes the mamebus.c code along with example setup and processing functions that are used in MATLAB. See Moscoso et al. (2021) for additional model details.

References

Abernathey, R. P., & Marshall, J. (2013). Global surface eddy diffusivities derived from satellite altimetry. *Journal of Geophysical Research: Oceans*, *118*(2), 901-916.

Albert, A., Echevin, V., Lévy, M., & Aumont, O. (2010). Impact of nearshore wind stress curl on coastal circulation and primary productivity in the peru upwelling system. *Journal of Geophysical Research: Oceans*, *115*(C12).

Amante, C., & Eakins, B. W. (2009). Etopo1 arc-minute global relief model: procedures, data sources and analysis.

Andersen, K., Berge, T., Goncalves, R., Hartvig, M., Heuschele, J., Hylander, S., ... Kiorboe, T. (2016). Characteristic sizes of life in the oceans, from bacteria to

whales. *Annual Review of Marine Science*, *8*(1), 217-241.

Armstrong, R. A. (1994). Grazing limitation and nutrient limitation in marine ecosystems: steady state solutions of an ecosystem model with multiple food chains. *Limnology and Oceanography*, *39*(3), 597–608.

Bakun, A., & Nelson, C. S. (1991). The Seasonal Cycle of Wind-Stress Curl in Subtropical Eastern Boundary Current Regions. *J. Phys. Oc.*, *21*(12), 1815-1834.

Bakun, A., & Parrish, R. H. (1982). Turbulence, Transport, and Pelagic Fish in the California and Peru Current Systems. *CalCOFI Rep.*, *23*.

Banas, N. S. (2011). Adding complex trophic interactions to a size-spectral plankton model: Emergent diversity patterns and limits on predictability. *Ecol. Modeling*, *222*, 2663–2675.

Botsford, L. W., Lawrence, C. A., Dever, E. P., Hastings, A., & Largier, J. (2006). Effects of variable winds on biological productivity on continental shelves in coastal upwelling systems. *Deep Sea Research Part II: Topical Studies in Oceanography*, *53*(25-26), 3116–3140.

Brandini, F. P., Nogueira Jr, M., Simião, M., Codina, J. C. U., & Noernberg, M. A. (2014). Deep chlorophyll maximum and plankton community response to oceanic bottom intrusions on the continental shelf in the south brazilian bight. *Continental Shelf Research*, *89*, 61–75.

Capet, X., Colas, F., McWilliams, J., Penven, P., & Marchesiello, P. (2008). Eddies in eastern boundary subtropical upwelling systems. *Ocean Modeling in an Eddying Regime, Geophys. Monogr. Ser*, *177*, 131–147.

Capet, X., Marchesiello, P., & McWilliams, J. (2004). Upwelling response to coastal wind profiles. *Geophysical Research Letters*, *31*(13).

Castelao, R. M., & Luo, H. (2018). Upwelling jet separation in the california current system. *Scientific Reports*, *8*(1).

Chavez, F. P., & Messié, M. (2009). A comparison of eastern boundary upwelling ecosystems. *Prog. in Oceanog.*, *83*, 80–96.

Cheresh, J., & Fiechter, J. (2020). Physical and biogeochemical drivers of alongshore ph and oxygen variability in the california current system. *Geophysical Research Letters*, *47*(19), e2020GL089553.

Colas, F., Capet, X., Mcwilliams, J. C., & Li, Z. (2013). Mesoscale Eddy Buoyancy Flux and Eddy-Induced Circulation in Eastern Boundary Currents. *J. Phys. Oc.*, *43*.

Colas, F., McWilliams, J. C., Capet, X., & Kurian, J. (2012). Heat balance and eddies in the peru-chile current system. *Climate dynamics*, *39*(1), 509–529.

Connolly, T. P., Hickey, B. M., Shulman, I., & Thomson, R. E. (2014). Coastal trapped waves, alongshore pressure gradients, and the california undercurrent. *Journal of Physical Oceanography*, *44*(1), 319-342.

Cullen, J. J. (1982). The deep chlorophyll maximum: comparing vertical profiles of chlorophyll a. *Canadian Journal of Fisheries and Aquatic Sciences*, *39*(5), 791–803.

Dauhajre, D. P., & McWilliams, J. C. (2018). Diurnal evolution of submesoscale front and filament circulations. *Journal of Physical Oceanography*, *48*(10), 2343-2361.

Deutsch, C., Frenzel, H., McWilliams, J. C., Renault, L., Kessouri, F., Howard, E., ... Yang, S. (2021). Biogeochemical variability in the california current system. *Progress in Oceanography*, *196*, 102565.

Di Lorenzo, E. (2003). Seasonal dynamics of the surface circulation in the southern california current system. *Deep Sea Research Part II: Topical Studies in Oceanography*, *50*(14-16), 2371–2388.

Eppley, R., Rogers, J., & McCarthy, J. (1969). Half-saturation constants for uptake of nitrate and ammonium by marine phytoplankton. *Limnology and Oceanography*, *17*, 912—920.

Ferrari, R., McWilliams, J. C., Canuto, V. M., & Dubovikov, M. (2008). Parameterization of eddy fluxes near oceanic boundaries. *J. Climate*, *21*(12), 2770–2789.

Fiechter, J., Edwards, C. A., & Moore, A. M. (2018). Wind, circulation, and topographic effects on alongshore phytoplankton variability in the california current. *Geophysical Research Letters*, *45*(7), 3238–3245.

Follows, M. J., & Dutkiewicz, S. (2011). Modeling diverse communities of marine microbes. *Annual review of marine science*, *3*, 427–451.

García-Reyes, M., Largier, J. L., & Sydeman, W. J. (2014). Synoptic-scale upwelling indices and predictions of phyto-and zooplankton populations. *Progress in Oceanography*, *120*, 177–188.

Gent, P. R., & McWilliams, J. C. (1990). Isopycnal mixing in ocean circulation models. *J. Phys. Oceanogr.*, *20*(1), 150–155.

Goebel, N. L., Edwards, C. A., Zehr, J. P., & Follows, M. J. (2010). An emergent community ecosystem model applied to the california current system. *Journal of Marine Systems*, *83*(3-4), 221–241.

Golden, C. D., Allison, E. H., Cheung, W. W., Dey, M. M., Halpern, B. S., McCauley, D. J., ... Myers, S. S. (2016). Nutrition: Fall in fish catch threatens human health. *Nature News*, *534*(7607), 317.

Gruber, N., Frenzel, H., Doney, S. C., Marchesiello, P., McWilliams, J. C., Moisan, J. R., ... Stolzenbach, K. D. (2006). Eddy-resolving simulation of plankton ecosystem dynamics in the california current system. *Deep Sea Research Part I: Oceanographic Research Papers*, *53*(9), 1483–1516.

Gruber, N., et al. (2011). Eddy-induced reduction of biological production in eastern boundary upwelling systems. *Nat. Geosciences*, *4*.

Hansen, B., Bjornsen, P., & Hansen, P. (1994). The size ratio between planktonic predators and their prey. *Limnology and Oceanography*, *39*, 395–403.

Henson, S. A., Cael, B., Allen, S. R., & Dutkiewicz, S. (2021). Future phytoplankton diversity in a changing climate. *Nature communications*, *12*(1), 1–8.

Hersbach, H., Bell, B., Berrisford, P., Hirahara, S., Horányi, A., Muñoz-Sabater, J., ... others (2020). The era5 global reanalysis. *Quarterly Journal of the Royal Meteorological Society*, *146*(730), 1999–2049.

Hood, R. R., Abbott, M. R., & Huyer, A. (1991). Phytoplankton and photosynthetic light response in the coastal transition zone off northern california in june 1987. *Journal of Geophysical Research: Oceans*, *96*(C8), 14769–14780.

Huisman, J., van Oostveen, P., & Weissing, F. J. (1999). Critical depth and critical turbulence: two different mechanisms for the development of phytoplankton blooms. *Limnology and oceanography*, *44*(7), 1781–1787.

Jacox, M., & Edwards, C. (2012). Upwelling source depth in the presence of nearshore wind stress curl. *J. Phys. Resc.*, *117*.

Jacox, M. G., Edwards, C. A., Hazen, E. L., & Bograd, S. J. (2018). Coastal upwelling revisited: Ekman, bakun, and improved upwelling indices for the us west coast. *Journal of Geophysical Research: Oceans*, *123*(10), 7332–7350.

Jacox, M. G., Hazen, E. L., & Bograd, S. J. (2016). Optimal environmental conditions and anomalous ecosystem responses: Constraining bottom-up controls of phytoplankton biomass in the california current system. *Scientific Reports*, *6*(1), 27612.

Jacox, M. G., Moore, A. M., Edwards, C. A., & Fiechter, J. (2014). Spatially resolved upwelling in the California Current System and its connections to climate variability. *Geophys. Res. Lett.*, *41*.

Jacox, M. J., & Edwards, C. A. (2011). Effects of stratification and shelf slope on nutrient supply in coastal upwelling regions. *Journal of Geophysical Research: Oceans*, *116*(C3).

Karl, D. M. (2002). Nutrient dynamics in the deep blue sea. *TRENDS in Microbiology*, *10*(9), 410–418.

Kessouri, F., Bianchi, D., Renault, L., McWilliams, J. C., Frenzel, H., & Deutsch, C. A. (2020). Submesoscale currents modulate the seasonal cycle of nutrients and productivity in the california current system. *Global Biogeochemical Cycles*, *34*(10), e2020GB006578.

Kiørboe, T. (2011). How zooplankton feed: mechanisms, traits and trade-offs. *Biological reviews*, *86*(2), 311–339.

Kriest, I. (2002). Different parameterizations of marine snow in a 1d-model and their influence on representation of marine snow, nitrogen budget and sedimentation. *Deep Sea Research Part I: Oceanographic Research Papers*, *49*(12), 2133–2162.

Lacasce, J. H. (2017). The prevalence of oceanic surface modes. *Geophysical Research Letters*, *44*(21), 11–097.

Lentz, S. J., & Chapman, D. C. (2004). The importance of nonlinear cross-shelf momentum flux during wind-driven coastal upwelling. *Journal of Physical Oceanography*, *34*(11), 2444–2457.

Lentz, S. J., & Fewings, M. R. (2012). The wind-and wave-driven inner-shelf circulation. *Annual review of marine science*, *4*, 317–343.

Loeuille, N., & Loreau, M. (2005). Evolutionary emergence of size-structured food webs. *Proceedings of the National Academy of Sciences*, *102*(16), 5761–5766.

Mahadevan, A., D'asaro, E., Lee, C., & Perry, M. J. (2012). Eddy-driven stratification initiates north atlantic spring phytoplankton blooms. *Science*, *337*(6090), 54–58.

Marañón, E., Cermeño, P., Huete-Ortega, M., López-Sandoval, D. C., Mouriño-Carballido, B., & Rodríguez-Ramos, T. (2014). Resource supply overrides temperature as a controlling factor of marine phytoplankton growth. *PloS one*, *9*(6), e99312.

Messié, M., Ledesma, J., Kolber, D. D., Michisaki, R. P., Foley, D. G., & Chavez, F. P. (2009). Potential new production estimates in four eastern boundary upwelling ecosystems. *Progress in Oceanography*, *83*(1-4), 151–158.

Moscoso, J. E., Bianchi, D., & Stewart, A. L. (2022). Controls and characteristics of biomass quantization in size-structured planktonic ecosystem models. *Ecological Modelling*, *468*, 109907.

Moscoso, J. E., Stewart, A. L., Bianchi, D., & McWilliams, J. C. (2021). The meridionally averaged model of eastern boundary upwelling systems (mamebusv1. 0). *Geoscientific Model Development*, *14*(2), 763–794.

Negrete-García, G., Luo, J. Y., Long, M. C., Lindsay, K., Levy, M., & Barton, A. D. (2022). Plankton energy flows using a global size-structured and trait-based model. *bioRxiv*.

Obata, A., Ishizaka, J., & Endoh, M. (1996). Global verification of critical depth theory for phytoplankton bloom with climatological in situ temperature and satellite ocean color data. *Journal of Geophysical Research: Oceans*, *101*(C9), 20657–20667.

Perlin, A., Moum, J., & Klymak, J. (2005). Response of the bottom boundary layer over a sloping shelf to variations in alongshore wind. *Journal of Geophysical Research: Oceans*, *110*(C10).

Polimene, L., Sailley, S., Clark, D., Mitra, A., & Allen, J. I. (2017). Biological or microbial carbon pump? the role of phytoplankton stoichiometry in ocean carbon sequestration. *Journal of Plankton Research*, *39*(2), 180–186.

Poulin, F. J., & Franks, P. J. (2010). Size-structured planktonic ecosystems: constraints, controls and assembly instructions. *Journal of plankton research*, *32*(8), 1121–1130.

Pozo Buil, M., Jacox, M. G., Fiechter, J., Alexander, M. A., Bograd, S. J., Curchitser, E. N., ... Stock, C. A. (2021). A dynamically downscaled ensemble of future projections for the california current system. *Frontiers in Marine Science*, *8*, 324.

Redi, M. H. (1982). Oceanic isopycnal mixing by coordinate rotation. *J. Phys. Oceanogr.*, *12*(10), 1154–1158.

Renault, L., Deutsch, C., McWilliams, J., Frenzel, H., Liang, J., & Colas, F. (2016). Partial decoupling of primary productivity from upwelling in the California Current system. *Nat. Geo. Sci.*, *9*, 505–510.

Rykaczewski, R. R., & Checkley, D. M. (2008). Influence of ocean winds on the pelagic ecosystem in upwelling regions. *Proceedings of the National Academy of Sciences*, *105*(6), 1965–1970.

Rykaczewski, R. R., & Dunne, J. P. (2010). Enhanced nutrient supply to the California Current Ecosystem with global warming and increased stratification in an earth system model. *Geo. Res. Lett.*, *37*.

Ryther, J. H. (1969). Photosynthesis and fish production in the sea: The production of organic matter and its conversion to higher forms of life vary throughout the world ocean. *Science*, *166*(3901), 72–76.

Sarmiento, J. L., & Gruber, N. (2006). *Ocean biogeochemical dynamics*. Princeton University Press.

Sauterey, B., Ward, B., Rault, J., Bowler, C., & Claessen, D. (2017). The implications of eco-evolutionary processes for the emergence of marine plankton community biogeography. *The American Naturalist*, *190*(1), 116–130.

Sheldon, R., Prakash, A., & Sutcliffe Jr, W. (1972). The size distribution of particles in the ocean 1. *Limnology and oceanography*, *17*(3), 327–340.

Skamarock, W. C., Klemp, J. B., Dudhia, J., Gill, D. O., Barker, D. M., Duda, M. G., ... others (2008). A description of the advanced research wrf version 3. *NCAR technical note*, *475*, 113.

Spellerberg, I. F., & Fedor, P. J. (2003). A tribute to claude shannon (1916–2001) and a plea for more rigorous use of species richness, species diversity and the 'shannon–wiener'index. *Global ecology and biogeography*, *12*(3), 177–179.

Stewart, A. L., & Moscoso, J. E. (2020). *A meridionally averaged model of eastern boundary upwelling systems (mamebusv1.0)*. Zenodo. (software) doi: https://doi.org/10.5281/zenodo.3866652

Stock, C. A., John, J. G., Rykaczewski, R. R., Asch, R. G., Cheung, W. W., Dunne, J. P., ... Watson, R. A. (2017). Reconciling fisheries catch and ocean productivity. *Proceedings of the National Academy of Sciences*, *114*(8), E1441–E1449.

Sverdrup, H. (1953). On conditions for the vernal blooming of phytoplankton. *J. Cons. Int. Explor. Mer*, *18*(3), 287–295.

Swenson, M. S., & Niiler, P. P. (1996). Statistical analysis of the surface circulation of the california current. *Journal of Geophysical Research: Oceans*, *101*(C10), 22631–22645.

Tang, E. (1995). The allometry of algal growth rates. *Journal of Plankton Research*, *17*, 1325–1335.

Taylor, A. G., Goericke, R., Landry, M. R., Selph, K. E., Wick, D. A., & Roadman, M. J. (2012). Sharp gradients in phytoplankton community structure across a frontal zone in the california current ecosystem. *Journal of Plankton Research*, *34*(9), 778–789.

Towns, J., Cockerill, T., Dahan, M., Foster, I., Gaither, K., Grimshaw, A., ... Wilkins-Diehr, N. (2014, Sept). XSEDE: Accelerating scientific discovery. *Computing in Science Engineering*, *16*(5), 62-74. doi: 10.1109/MCSE.2014.80

Tréguer, P., Bowler, C., Moriceau, B., Dutkiewicz, S., Gehlen, M., Aumont, O., ... others (2018). Influence of diatom diversity on the ocean biological carbon pump. *Nature Geoscience*, *11*(1), 27–37.

Trowbridge, J., & Lentz, S. (1998). Dynamics of the bottom boundary layer on the northern california shelf. *Journal of Physical Oceanography*, *28*(10), 2075–2093.

Vallina, S. M., Follows, M., Dutkiewicz, S., Montoya, J. M., Cermeno, P., & Loreau, M. (2014). Global relationship between phytoplankton diversity and productivity

in the ocean. *Nature communications*, *5*(1), 1–10.

Van Oostende, N., Dussin, R., Stock, C., Barton, A., Curchitser, E., Dunne, J., & Ward, B. (2018). Simulating the ocean's chlorophyll dynamic range from coastal upwelling to oligotrophy. *Progress in oceanography*, *168*, 232–247.

Ward, B. A., Dutkiewicz, S., Jahn, O., & Follows, M. J. (2012). A size-structured food-web model for the global ocean. *Luminol. Oceanogr.*, *57*(6), 1877–1891.

Worden, A. Z., Nolan, J. K., & Palenik, B. (2004). Assessing the dynamics and ecology of marine picophytoplankton: the importance of the eukaryotic component. *Limnology and oceanography*, *49*(1), 168–179.

Zubkov, M. V., Sleigh, M. A., & Burkill, P. H. (2000). Assaying picoplankton distribution by flow cytometry of underway samples collected along a meridional transect across the atlantic ocean. *Aquatic Microbial Ecology*, *21*(1), 13–20.